学位論文

Doctor's Thesis

Myocardial perfusion and function with a combined SPECT/CT system

(SPECT/CTシステムによる心筋血流と機能評価)

宇都宮　大輔

Daisuke Utsunomiya

熊本大学院医学研究科博士課程内科系専攻放射線医学

指導：山下　康行教授

2006 年 3 月

学位論文

Doctor's Thesis

論文題名　：Myocardial perfusion and function with a combined SPECT/CT system
（SPECT/CTシステムによる心筋血流と機能評価）

著者名　　：　宇都宮　大輔
Daisuke Utsunomiya

指導教員名：　山下　康行　教授

審査委員名：　生体機能薬理学担当教授　　光山　勝慶

放射線治療医学担当教授　　大屋　夏生

心臓血管外科学担当教授　　川筋　道雄

形態構築学担当教授　　児玉　公道

2006年3月

Myocardial perfusion and function with a combined SPECT/CT system

Contents

Syllabus

Spatially registered single photon emission computed tomography (SPECT) and computed tomography (CT) images can be used to correlate physiological information from the SPECT emission image with anatomical information from the CT transmission image. The CT data also can be used to generate an attenuation map to correct attenuation errors in the SPECT image. One application for which this attenuation correction is critical is cardiac perfusion assessment, in which attenuation errors are often difficult to distinguish from perfusion defects.

Current emission-transmission systems capable of producing spatially registered SPECT and CT images typically use a radionuclide source to acquire the transmission data. The limited photon flux of the radionuclide source compromised both spatial resolution and image statistics, and prolongs acquisition of the transmission data. Another approach is to obtain emission and transmission data with separate imaging systems. This approach complicates image registration, especially in the thorax, since the patient is moved between two image acquisitions. The imaging system that combines a gantry-free gamma camera with multidetector-row CT (MDCT) allows for accurate image registration between SPECT and CT. Using this combined SPECT/CT imaging system, we aimed the optimization and clinical application of X-ray CT based attenuation correction of myocardial SPECT imaging. Furthermore, we compared results of left ventricular (LV) function obtained by quantitative gated single-photon emission tomography (QGS) and MDCT with reference parameters using an cardiac physical phantom.

Section 1. Object-specific attenuation correction of the thorax.

The purpose of this section was to prospectively evaluate the breathing

conditions for patients. during a CT scan, that resulted in the best match with SPECT imaging of the thorax. The registration errors between myocardial SPECT and CT images under different protocols (normal inhalation [NI], normal exhalation [NE] and free-breathing [FB]) were compared. Thirteen normal subjects were studied. CT scans matched better with SPECT images during FB and NE than during NI (one-way analysis of variance, $P < 0.01$). The percentages with registration artifacts using internal landmarks (31 %, 15 % and 8 %, respectively, under NI, NE and FB) were smaller than those using external markers (69 %, 31 % and 15 %, respectively, under NI, NE and FB). Internal registration and the use of free-breathing or exhalation protocols are recommended for attenuation correction.

Section 2. Clinical application of X-ray CT based attenuation correction in myocardial perfusion SPECT imaging

Attenuation artifacts adversely affect the diagnostic accuracy of myocardial perfusion imaging. We assessed the clinical usefulness of X-ray CT based attenuation correction in patients undergoing myocardial perfusion imaging by comparing their myocardial attenuation corrected- and non-corrected SPECT images with the coronary angiography (CAG). We retrospectively reviewed the myocardial SPECT images of 30 patients (18 men, 12 women; mean age 68 years). 13 of 30 patients with coronary artery disease (CAD) and 17 without CAD were confirmed by CAG. They underwent sequential CT and myocardial SPECT imaging with thallium-201 (111 MBq) under an exercise or pharmacological stress protocol using our combined SPECT/CT system. Two readers reviewed the myocardial SPECT images for the presence of CAD on a 4-point scale where 1 = normal, 2 = probably normal. 3 = probably abnormal, and 4 = abnormal. Two reading sessions were held. First, non-corrected SPECT and second, attenuation-corrected SPECT images using X-ray CT images were interpreted. Interobserver variability was assessed with kappa

statistics. Diagnostic performance (accuracy) of coronary arterial stenosis was compared between attenuation-corrected and non-corrected images. Interobserver agreement for visual assessment was substantial or almost perfect. For attenuation-corrected images, the observer consensus for analysis was 0.84 for the LAD-, 0.87 for the LCX-, and 0.71 for the RCA-territory. For non-corrected images, it was 0.91, 0.71, and 0.78. Attenuation correction resulted in statistically significant improvements in overall diagnostic accuracy (sensitivity/specificity/accuracy = 76%/93%/89%, 67%/86%/81%, respectively, for attenuation-corrected and NC-images). Because of an increase in the specificity, diagnostic accuracy was significantly increased on attenuation-corrected images. These data suggest that X-ray CT based attenuation correction in myocardial SPECT imaging has the potential to develop into a reliable clinical technique.

Section 3. MDCT and QGS for the assessment of LV function

The purpose of this section was to compare results of left ventricular (LV) function obtained by quantitative gated single-photon emission tomography (QGS) and MDCT with reference parameters using an electrocardiogram-gated cardiac physical phantom. The phantom study was performed using a combined SPECT/CT system. Flexible membranes formed the inner and outer walls of the simulated LV. The stroke volume was adjusted (45mL or 58mL) and the fixed 42-mL end-systolic volume (ESV) produced two different volume combinations. The LV function parameters were estimated by means of MDCT and QGS. Differences in true and measured volumes were compared among CT with a reconstructed image thickness of 2.5mm and 5.0mm and QGS volumetric values. Each scan was repeated three-times. The estimation of LV volumes using both QGS and MDCT analyses were reproducible very well. QGS overestimated ejection fraction (EF) by approximately 20%; MDCT volumetry overestimated EF by approximately 5% in each volume

setting. The differences in true and measured values for EF and ESV obtained with QGS were significantly greater than obtained with MDCT. In conclusion, MDCT provides a reliable estimation of functional LV parameters, whereas QGS tends to significantly overestimate the EF in small hearts.

Associated Articles

1. Utsunomiya D, Nakaura T, Honda T, Shiraishi S, Tomiguchi S, Kawanaka K, Morishita S, Awai K, Ogawa H, Yamashita Y.

Object-specific attenuation correction at SPECT/CT in thorax: optimization of respiratory protocol for image registration

Radiology 237: 662-669, 2005.

2. Utsunomiya D, Tomiguchi S, Shiraishi S, Yamada K, Honda T, Kawanaka K, Kojima A, Awai K, Yamashita Y.

Initial experience with X-ray CT based attenuation correction in myocardial perfusion SPECT imaging using a combined SPECT/CT system.

Annals of Nuclear Medicine 19: 485-489, 2005.

3. Utsunomiya D, Tomiguchi S, Awai K, Shiraishi S, Nakaura T, Yamashita Y.

Mutidetector-row CT and quantitative gated SPECT for the assessment of left ventricular function in small hearts: the cardiac physical phantom study using a combined SPECT/CT system.

European Radiology published online February 3, 2006.

Other Articles

1. Utsunomiya D. Notsute S, Hayashida Y. Lwakatare F, Katabuchi H. Okamura H, Awai K, Yamashita Y.

Endometrial carcinoma in adenomyosis: assessment of myometrial invasion on T2-weighted spin-echo and gadolinium-enhanced T1-weighted images.

American Journal of Roentgenology 182: 399-404, 2004.

2. Utsunomiya D, Shiraishi S, Imuta M, Tomiguchi S. Morishita S, Awai K, Yamashita Y.

Added value of SPECT/CT fusion in assessing suspected bone metastasis: comparison with scintigraphy alone and nonfused scintigraphy and CT.

Radiology 238: 264-271, 2006.

3. Utsunomiya D. Awai K, Tamura Y, Nishiharu T, Urata J, Sakamoto T, Taniguchi A, Yamashita Y. 16-MDCT aortography with a low-dose contrast material protocol.

American Journal of Roentgenology 186: 374-378, 2006.

4. Nakaura T, Utsunomiya D, Shiraishi S, Tomiguchi S, Honda T, Ogawa H, Awai K, Yamashita Y.

Three-dimensional cardiac image fusion using new CT angiography and SPECT methods.

American Journal of Roentgenology 185: 1554-1557, 2005.

5. Utsunomiya D, Nakaura T, Tomiguchi S, Shiraishi S, Kawanaka K, Katsuda N, Awai K, Yamashita Y.

Anatomical and functional imaging in cardiology: the path to cardiac image fusion.

Nichidoku-iho 50: 351-357, 2005.

Abbreviations

ANOVA: analysis of variance

CAD: coronary artery disease

CAG: coronary angiography

CoV: coefficient of variance

ECG: electrocardiogram

EDV: end-diastolic volume

EF: ejection fraction

ESV: end-systole volume

FB: free-breathing

LAD: left anterior descending artery

LCX: left circumflex artery

LV: left ventricle

MDCT: multidetector-row CT

ML-EM: maximum likelihood expectation maximization

NE: normal exhalation

NI: normal inhalation

QGS: quantitative gated single-photon emission tomography

RCA: right coronary artery

ROI: region of interest

SD: standard deviation

SPECT: single photon emission computed tomography

TCT: transmission computed tomography

Tl-201: thallium-201

Section 1. Object-specific attenuation correction of the thorax

Cardiac single photon emission computed tomography (SPECT) has become widely used as a non-invasive procedure for the examination of myocardial perfusion. In SPECT imaging, however, photon attenuation correction is important, due to nonuniform distributions of attenuation coefficients (1-6). An attenuation correction method via the use of an attenuation map produced by X-ray computed tomography (CT) images has been proposed to counter this problem (7-9). For reliable attenuation correction, however, anatomically accurate image registration between SPECT and CT scans is vital. Recently, a gamma camera-mounted anatomical X-ray tomography has been introduced (7, 10). However, there are some drawbacks for such hybrid scanners. An important drawback is poorer performance of the X-ray-tube-based CT system. The lower-resolution CT images may be sufficient for attenuation correction, but often be insufficient for image interpretation in clinical circumstances. In order to create a robust mode for inherent registration between SPECT and high-resolution CT images, we have combined SPECT and MDCT scanners for accurate image fusion between SPECT and CT scans. In this system, imaging by both SPECT and CT can be performed sequentially, without the need to transfer the patient. Both attenuation correction and accurate localization of myocardial perfusion on high-resolution cardiac MDCT images is therefore possible, similar to integrated PET/CT scanner (10, 11). There are remaining potential registration errors in a combined system that can arise from physiological motions caused by breathing (12-15), but the assessment of the

influence of respiratory movement on attenuation correction using a combined functional/anatomical scanner has been the subject of only a few studies (12, 13). Thus, the aim of our study was to prospectively evaluate the breathing conditions for patients. during a CT scan, that resulted in the best match with SPECT imaging of the thorax.

MATERIALS AND METHODS

Subjects

Thirteen human subjects (seven males and six females) underwent a myocardial SPECT with 111MBq (3mCi) of thallium-201 (Tl-201) and three CT scans under different respiratory protocols. The median age was 58 years, with the ages ranging 33 to 80 years. The study group consisted of six normal healthy volunteers (four males and two females; age, 33-64 years old; median age, 50 years) and seven patients (three males and four females; age, 50-80 years old; median age, 62 years) without the history of coronary artery disease (CAD). Six volunteers were considered normal from their history, physical examination, and electrocardiogram. Seven consecutive patients were referred for rest myocardial SPECT imaging presented with atypical chest pain during the period between November 2002 and January 2003. Each of the seven patients subsequently underwent echocardiography and coronary angiography (CAG) which revealed no evidence of CAD, and they were therefore considered normal.

Respiratory protocols

All subjects underwent three CT scans under free-breathing (FB) conditions, followed by CT scans whilst holding their breath at normal inhalation (NI) and also at normal exhalation (NE). NI was defined as the respiratory level that was reached when the subjects first inhaled, without forcing inhalation, and then held their breaths. NE

was defined as the respiratory level that was reached when the subjects first inhaled and then exhaled, without forcing exhalation, and then held their breaths.

System Overview

Our combined SPECT/CT system incorporates a SPECT scanner and a MDCT scanner, both of which are commercially available instruments (Fig.1a, b). The gantry-free SPECT system used was a Skylight (ADAC Laboratories, Milpitas, CA). The eight-detector-row MDCT scanner was a LightSpeed Ultra (General Electric Medical System, Milwaukee, Wis). The SPECT system and CT scanner were positioned so that the extended CT table could move the patient directly into the SPECT scanner.

SPECT imaging

Dual-head detectors were equipped with low energy, general-purpose (LEGP) parallel-hole collimators with the heads oriented at 90 degrees to each other. The 35% window was centered at about 74 keV for the emission data and projections were digitized onto a 64 x 64 matrix and 41-cm scan field of view. A total of 32 projections were sampled over 90 degrees for each detector and each view was acquired for 60 seconds. SPECT images were reconstructed by filtered back projection and high frequency noise levels were decreased with post-reconstruction Butterworth filtering (cutoff = 0.50 cycle/pixel, order = 5) on a Pegasys workstation (ADAC Laboratories, Milpitas, CA). Images were then displayed as axial, coronal, and sagittal views for image registration. Images were also displayed as cardiac views (horizontal and vertical long-axis and short-axis slices).

CT imaging

Based on the results of the preliminary study described in the appendix section, we adopted a low-current CT protocol for X-ray CT based attenuation correction. CT scans

under NI and NE protocols were performed in a helical mode with a 0.7-second rotation time, 8 x 2.5 mm collimation, 120 kV and 10 mA. The scan was reconstructed at 5-mm section thickness. In order to make a CT scan under FB protocol an average image generated over a breathing cycle and avoid imaging of the diaphragm at different positions. we selected a slow rotation time. CT scans under the FB protocol were performed in an incremental mode with a 4 sec rotation time, 5.0-mm detector-row width. 5.0-mm image thickness, 140 kV and 10 mA. CT images were reconstructed by a standard reconstruction algorithm with a 512 x 512 matrix and 50-cm scan field of view. CT dose index (vol) was 1.0 mGy and 3.4 mGy, respectively , for NI/NE protocol and FB protocol.

Registration method between SPECT and CT

SPECT and CT image registration was performed by two different methods. First, semi-automated registration (external registration) was performed by means of external markers (three-port cocks with locks made of polycarbonate) in which two external markers containing an aqueous solution of Tl-201 and contrast medium were attached to the cushion of the imaging table. Second, manual registration was performed by use of the heart border as an internal marker (internal registration). The validity of the image registration was evaluated on the computer display by consensus between two diagnostic radiologists. One had eight years experience, and the other had 20 years experience in both CT and cardiac SPECT imaging.

Use of CT Images for Attenuation Correction

Attenuation correction using CT images was performed by use of specifically developed software (HYOGO CM Attenuation Correction, Hyogo College of Medicine. Nishinomiya, Hyogo) on a Pegasys workstation (7). A flowchart describing the process

is shown in Figure 2. Registration of SPECT and CT images was performed on a Pegasys workstation. CT data were retrieved from an Advantage Windows 4.0P workstation (General Electric Medical System, Milwaukee, Wis) and then converted to a SPECT-like data volume (5.9mm x 5.9mm x 5.9mm) for registration of the SPECT and CT images. After CT and SPECT image registration, the CT number was converted to the attenuation coefficients (μ) corresponding to the X-ray energy of 74keV by linearly scaling. The following equation was used for the relationship between CT number and μ (1/cm): μ=0.181 x (CT + 1000) / 1000.

The attenuation-corrected SPECT images were reconstructed with this attenuation coefficient map by means of a maximum-likelihood expectation-maximization (ML-EM) algorithm. Three SPECT images with attenuation correction, by using CT images under different respiratory protocols, were produced for each registration method. The transaxial slices were automatically reoriented to horizontal and vertical long-axis and short-axis slices and the reoriented reconstructed data sets and the Bull's eye display were then used for visual evaluation.

Measurements of registration error between SPECT and CT images

The gaps between the SPECT and CT data under the three different respiratory conditions were measured for each registration method. Reference points for registration were as follows: (a) the top of the diaphragm, (b) the left border of the heart and (c) the chest wall border (Fig.3). The coordinates in the x-, y-, z- axis of each reference point in CT and SPECT were investigated and three dimensional distances between the coordinate of reference points of CT and that of SPECT were calculated. All measurements were performed by an experienced radiologist who took preliminary

measurements in five additional subjects to optimize the techniques prior to this study. This radiologist had nine years experience in both CT and cardiac SPECT imaging.

Visual evaluation of the final attenuation-corrected SPECT images

Attenuation-corrected SPECT images using CT images under different respiratory protocols were presented to two observers on a computer display with a linear rainbow color scale with seven colors ranging from purple to red. One observer had seven years experience and the other had 10 years experience in cardiac SPECT imaging. Observers were aware that all the subjects were normal. Observers visually evaluated the attenuation-corrected SPECT images under the three respiratory protocols for the overall presence of artifactual radioactivity reduction and their location, which were then classified as either no artifact, mild activity reduction (artifactual wall thinness was up to 50%) or severe activity reduction (artifactual wall thinness was more than 50%). The location of designated artifacts was classified as either anterior, inferior, septal or lateral wall of myocardium. Visual evaluations were performed independently so as to determine interobserver agreement between two observers, including a physician and a radiologist. Where disagreements occurred, the more severe classification was accepted as the final determination.

Statistical Analysis

Before the study, a power analysis was performed by using preliminary registration error measurements obtained in five additional subjects who were not included in the final study population in order to determine sample size for statistical analysis. The differences of mean registration errors among respiratory protocols were approximately twofold greater than their standard deviations. Therefore, a minimum of 10 subjects

were considered appropriate for an intended power of 0.8 or greater at subsequent power analysis.

One-way analysis of variance (ANOVA) was used to test the statistical significance of the mean registration errors under the three respiratory protocols. If there were statistically significant differences, the Bonferroni-Dunn test was then used for post hoc analysis. P values of less than 0.01 were considered to be statistically significant. All data are represented as mean values ± standard deviations (SDs).

The degree of agreement between the two observers for visual evaluation of the attenuation-corrected SPECT images was measured with the kappa statistic. Kappa values were reported as follows: 0 = no agreement is a random effect; less than 0.20 = poor agreement; 0.21-0.40 = fair agreement; 0.41-0.60 = moderate agreement; 0.61-0.80 = substantial agreement; and 0.81-1.00 = almost perfect agreement (16). SAS 8.01 for Windows (SAS Institute, Cary, NC) was used for the statistical analyses. Power analysis was performed with commercially available free software (G-Power version 2.1.2; Axel Buchner et al. Available at: www.psycho.uni-duesseldorf.de/aap/projects/gpower/index.html).

RESULTS

Measurement of registration error between SPECT and CT images

The mean distances ± SDs between the reference points of the SPECT and CT images, under our three respiration protocols, for external registration are shown in Table 1. In external registration, statistical analysis using ANOVA revealed that matching of the diaphragm and the heart border, between the SPECT and CT images, gave statistically significant differences for different respiratory protocols. Post hoc analysis also revealed that matching of SPECT and CT images of the diaphragmatic dome and the heart border was statistically far better under the FB and NE protocols than that under the NI protocol (Table 2). The mean differences between the location of the diaphragmatic dome on the CT scan under FB, NE and NI and the location of the dome on the corresponding SPECT scan, were 5.56 mm ±7.55, -3.15 mm ±14.14, and 29.88 mm ± 5.37, respectively. The corresponding differences for the heart border were 8.57 mm ± 2.43, 13.30 mm ± 2.69, and 18.87 mm ±6.29, respectively.

The mean distances ± SDs between reference points of the SPECT and CT images, under our three respiration protocols, for internal registration are shown in Table 3. In internal registration, statistical analysis using ANOVA revealed that matching of the SPECT and CT images from the diaphragmatic dome and the chest wall border were significantly different between respiratory protocols and post hoc analysis revealed that these matches were significantly better under the FB and NE protocols than that under the NI protocol (Table 4). The mean differences in movement of the diaphragmatic dome on a CT scan under FB, NE and NI, as compared with its level on a SPECT scan, were 5.30 mm ± 4.32, -1.14 mm ± 9.92, and 24.16 mm ± 5.45, respectively. The corresponding differences of the chest wall border were 3.72 mm ± 3.08, 8.51 mm ±

5.03, and 20.60 mm ± 5.85, respectively.

Visual assessment of attenuation corrected SPECT images

Results of the visual assessment of attenuation-corrected SPECT images for each registration method are summarized in Tables 5 and 6. In external registration, the percentages with the presence of either mild or severe artifacts of decreased tracer activities were 69 % (9/13), 31 % (4/13), and 15 % (2/13) of all subjects under the NI, NE and FB protocols, respectively. In internal registration, the corresponding percentages were 31 % (4/13), 15 % (2/13), and 8 % (1/13) of all subjects, respectively, under the NI, NE and FB protocols (Fig.4). No severe artifacts were observed for either the NE or FB protocol. The method of image registration using internal landmarks (internal registration) therefore offered improved homogeneity in the display of apparent distribution of myocardial tracer uptake (Fig.5). In addition, no artifacts were observed in the septal and lateral walls for any of the subjects, using either registration method.

For each method of image registration, interobserver agreement (kappa statistic) in the visual evaluations was found to be either very high or perfect. For external registration, the observer consensus for analysis of the anterior myocardial wall was 0.876 for the NI protocol, 0.752 for the NE protocol and there was complete agreement for the FB protocol. The corresponding interobserver agreement for the inferior myocardial wall was 0.878, 0.828 and complete agreement, respectively. For internal registration, interobserver agreement when analyzing the anterior myocardial wall was 0.836 for the NI protocol there was complete agreement for both the NE and FB protocols. The corresponding consensus for the inferior myocardial wall was 0.821 for the NI protocol and there was complete agreement again for both the NE and FB

protocols.

DISCUSSION

Myocardial SPECT imaging with Tl-201 is a non-invasive, cost-effective and routinely available procedure that provides valuable prognostic information on the risk of future cardiac events for a wide spectrum of patients with known or suspected coronary artery disease (17-19). The diagnostic accuracy of myocardial SPECT is limited, however, by specific physical effects, including attenuation, scatter and blur (1-6) and among these perturbations, attenuation artifacts are arguably the most serious in the assessment of myocardial perfusion (6). Attenuation maps are commonly generated from monoenergetic transmission computed tomography images obtained using an external source (7, 9). This process, however, is not yet widely used in clinical practice due to low-quality transmission scan images resulting from low photon flux, the expense of both software and hardware and long scan times (7). Attenuation maps have also been generated from CT images (9). The quality of the final emission image that has been corrected for attenuation effects, largely depends on the registration of the transmission and emission imaging (20). Because a SPECT scan is an average image generated over many breathing cycles, fusion of SPECT images with CT images requires respiratory gating of the SPECT scans. We contend that this is not a good approach, however, owing to the substantial increases in imaging time that would result and that optimization of the image fusion therefore needs to focus on the CT data acquisition protocol.

This study showed that, for the combined SPECT/CT system, the accuracy of image registration was higher using both the FB and NE protocols during CT scanning

rather than the NI protocol. Attenuation-corrected SPECT images generated with the FB and NE protocols showed few artifacts and they were similarly homogenous for tracer uptake of Tl-201. Attenuation-corrected images under the NI protocol revealed artifacts of decreased tracer uptake, mimicking perfusion abnormalities, in the anterior and inferior wall. In the NI protocol, the attenuation of the heart itself and the diaphragm might well be underestimated due to registration errors between CT and SPECT images. We conclude therefore that CT images acquired during inhalation are not suitable for image fusion.

Goerres et al. (13) reported that the normal exhalation/breath-hold protocol for CT acquisition gave the best results in comparison with a free-breathing protocol for PET-CT image registration. In their study, data acquisition during FB was performed with a pitch of 1.7 - 2.5 and 5-mm section thicknesses in the helical mode. FB in the helical mode may introduce significant geometric uncertainties into the CT data (13, 21). For example, if the diaphragm moves superiorly or inferiorly between slice acquisition, the sequence of images may become disordered, with inferiorly indexed slices sampling superior positions of the structure (and vice versa) (13, 21). We considered that our FB protocol, using CT scanning with 4.0-second/rotation, in the incremental mode might normalize respiratory movements and reduce CT and SPECT image registration errors. Indeed, by using CT scanning with a 4.0-second/rotation setting during FB, imaging of the diaphragm at different positions leading to mushroom-shaped respiratory-induced artifacts could be completely avoided. An additional and important benefit of this was that FB could be performed by each of the patients, as for some subjects with coronary artery disease holding their breath can be quite difficult.

The quality of the final SPECT images with attenuation correction using an internal

landmark technique was higher than when using an external marker method and was hence more suitable for attenuation correction of myocardial SPECT images. The displacement of the heart between SPECT and CT images was quite high from image registration with external markers and this error caused artifactual perfusion abnormalities. We concluded, though, that displacement of the chest wall has little influence on the quality of the final attenuation corrected images.

This study has several limitations. First, the conversion from CT values to the attenuation coefficient of gamma rays is complicated as the energy spectrum of gamma rays is finite, whereas X-rays are continuous. Second, the SPECT images were not scatter-corrected which would improve image quality and accuracy of quantification. Third, SPECT images were generated with 180-degree data collection in this study which was chosen because the use of anterior 180-degree acquisition has become standardized in clinical use (22). Comparisons between 180 and 360-degree acquisitions were performed in both an anthropomorphic torso phantom and in one subject prior to this study and, by visual comparison, no significant differences were observed. Further studies are imperative to confirm these findings.

In conclusion, a SPECT and CT image registration method using an internal landmark and either a free-breathing or exhalation protocol for CT acquisition are recommended for proper object-specific attenuation correction of myocardial SPECT images.

APPENDIX

We had preliminarily investigated the optimal X-ray tube current for attenuation correction. High currents improve image quality but also increase radiation dose to the patient. If the CT scan is only to be used for attenuation correction, a low-current CT scan may be sufficient. We compared attenuation corrected SPECT images using low-current CT images (10 mA) with those using standard CT images (140 mA). The SPECT phantom (ECT QA Phantom type-JSP, Kyoto-kagaku, Kyoto, Japan) was used (Fig 6). Cylinder A, B, C, and D contained water, diluted contrast material at an iodine concentration of 10, 4.5, and 2.5 mgI/mL, respectively. The concentration of Tl-201 in each of four cylinders was 0.2 MBq/mL. Two unenhanced CT scans were acquired with 10 and 140 mA and in the following are designated CT 10 and CT 140, respectively. Two attenuation-corrected SPECT images ($SPECT_{CT10}$ and $SPECT_{CT140}$) by using CT images with different X-ray tube currents were produced using iterative reconstruction (Fig 7). The adequacy of the CT transmission maps was assessed by comparing measured counts of Tl-201 in regions of interest (ROIs) in each cylinder on two attenuation-corrected SPECT images. The size of each ROI was five pixels. To verify reproducibility of the phantom results, each scan was repeated seven times. Two-way ANOVA was used to evaluate the effect of CT current on attenuation-corrected SPECT images. The mean counts ± SDs in each cylinder on $SPECT_{CT10}$ and $SPECT_{CT140}$ images are shown in Table 7. There was no significant difference between the counts on $SPECT_{CT10}$ and $SPECT_{CT140}$ ($P = 0.95$). In summary, a low-current CT scan is sufficient for attenuation correction.

Table 1. CT and SPECT Image Registration Errors generated by external registration

	Diaphragm	Heart	Chest wall
	Mean ± SD	Mean ± SD	Mean ± SD
NI	29.88 ± 5.37	18.87 ± 6.29	5.60 ± 1.86
NE	-3.15 ± 14.14	13.30 ± 2.69	6.16 ± 2.06
FB	5.56 ± 7.55	8.57 ± 2.43	6.19 ± 1.75
P value	<0.01	<0.01	0.67

Note___ Data are represented by the mean (mm) ± standard deviation. P values were calculated for multiple comparisons. NI = normal inhalation, NE = normal exhalation, FB = free-breathing

Table 2. Post hoc analysis to compare means of the distances between CT and SPECT images generated by external registration

Diaphragm	P value	Heart	P value
NI vs NE	< 0.01	NI vs NE	< 0.01
NI vs FB	< 0.01	NI vs FB	< 0.01
NE vs FB	0.029	NE vs FB	< 0.01

Note___ NI = normal inhalation, NE = normal exhalation, FB = free-breathing

Table 3. CT and SPECT Image Registration Errors generated by internal registration

	Diaphragm	Heart	Chest wall
	Mean ± SD	Mean ± SD	Mean ± SD
NI	24.16 ± 5.45	0.00 ± 0.00	20.60 ± 5.85
NE	-1.14 ± 9.92	0.00 ± 0.00	8.51 ± 5.03
FB	5.30 ± 4.32	0.00 ± 0.00	3.72 ± 3.08
P value	< 0.01	1.00	< 0.01

Note___ Data are represented by the mean (mm) ± standard deviation. P values were calculated for multiple comparisons. NI = normal inhalation, NE = normal exhalation, FB = free-breathing

Table 4. Post hoc analysis to compare means of the distances between CT and SPECT images generated by internal registration.

Diaphragm	P value	Chest wall	P value
NI vs NE	< 0.01	NI vs NE	< 0.01
NI vs FB	< 0.01	NI vs FB	< 0.01
NE vs FB	0.025	NE vs FB	0.016

Note___ NI = normal inhalation, NE = normal exhalation, FB = free-breathing

Table 5. Visual evaluation of final attenuation-corrected SPECT images by external registration.

		No	Mild	Severe
NI	Anterior	5	4	4
	Inferior	4	3	6
NE	Anterior	10	3	0
	Inferior	9	3	1
FB	Anterior	11	2	0
	Inferior	11	2	0

Note ___ No = No artifact, Mild = Mild artifact, Severe = Severe artifact
NI = normal inhalation, NE = normal exhalation, FB = free-breathing
Anterior = anterior wall of myocardium, Inferior = inferior wall of myocardium

Table 6. Visual evaluation of final attenuation-corrected SPECT images by internal registration

		No	Mild	Severe
NI	Anterior	10	1	2
	Inferior	9	2	2
NE	Anterior	11	2	0
	Inferior	13	0	0
FB	Anterior	12	1	0
	Inferior	13	0	0

Note___No = no artifact, Mild = mild artifact, Severe = severe artifact
NI = normal inhalation protocol, NE = normal exhalation protocol, FB = free-breathing protocol
Anterior = anterior wall of myocardium, Inferior = inferior wall of myocardium

Table 7. The mean counts ± SDs in each cylinder on $SPECT_{CT10}$ and $SPECT_{CT140}$.

	A	B	C	D
$SPECT_{CT10}$	9021 ± 1577	8935 ± 1250	8642 ± 714	8935 ± 1124
$SPECT_{CT140}$	8979 ± 1570	8871 ± 1126	8671 ± 714	8933 ± 1119

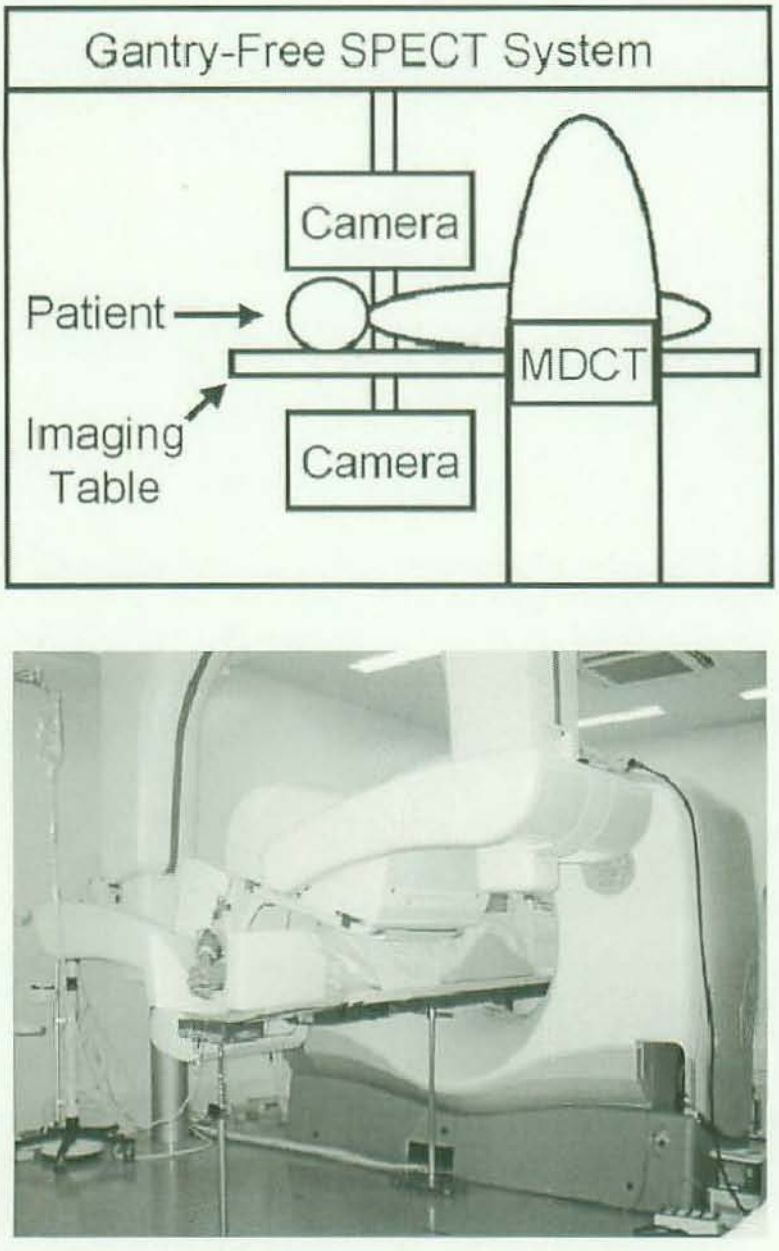

Fig.1. Schematic (upper) and photograph (lower) representation of our combined SPECT/CT system with adjacent SPECT and CT scanners that do not require repositioning of the patient as the patient table from the CT scanner extends into the gantry-free SPECT system.

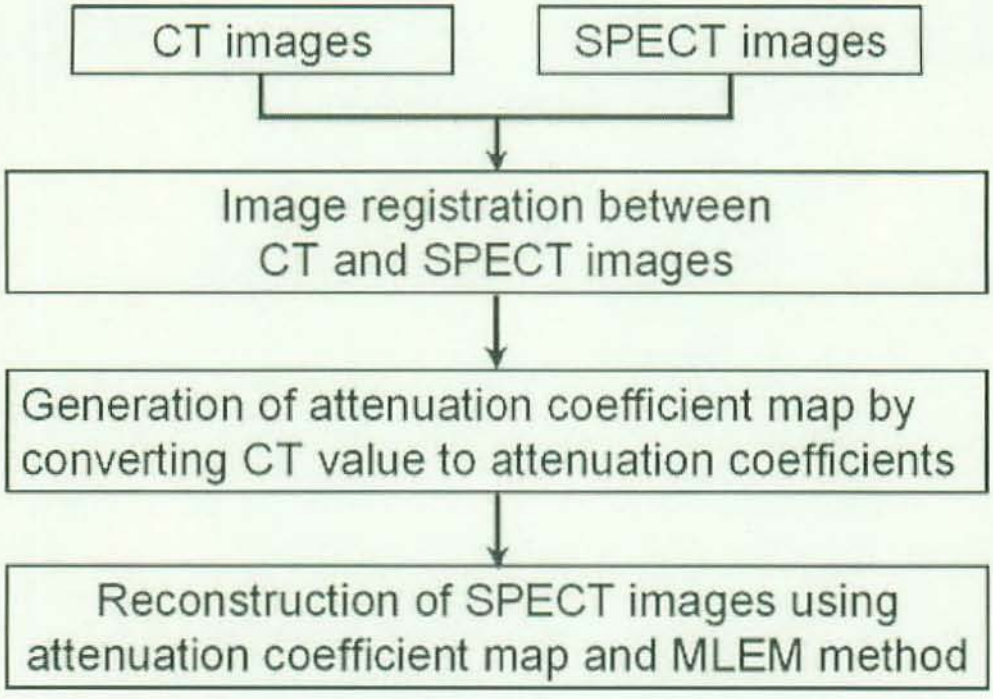

Fig.2. Flowchart of the process of attenuation correction using CT images

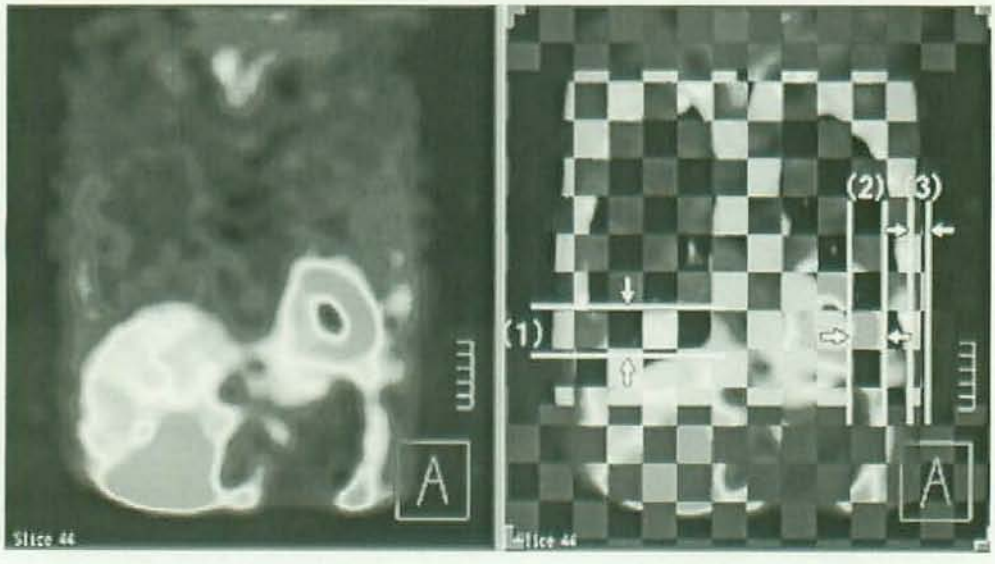

Fig 3. Coronal fusion image for measurement of the distances between the following reference points of both SPECT and CT images: (1) diaphragmatic dome, (2) heart border, (3) chest wall border.

Fig 4. a **b** **c**

Final attenuation-corrected short-axial SPECT images of a 32-year-old man generated using three respiratory protocols by internal registration. (a) Severe decreased tracer uptake artifact was observed in the inferior wall under NI (arrows). The attenuation corrected images under the NE (b) and FB (c) showed no artifacts.

Note ___ NI = normal inhalation protocol, NE = normal exhalation protocol, FB = free-breathing protocol.

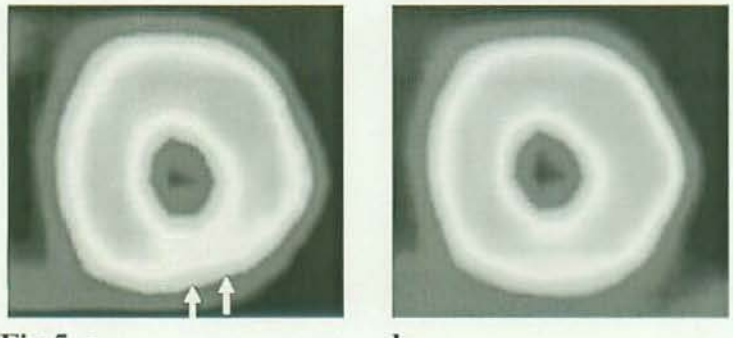

Fig 5. a **b**

Final attenuation-corrected short-axial SPECT images of 60-year-old man generated under NI by external (a) and internal registration (b). (a) Severe decreased tracer uptake artifacts were observed in the inferior wall by external registration (arrows). (b) No artifacts were observed under the internal registration.

Note ___ NI = normal inhalation protocol.

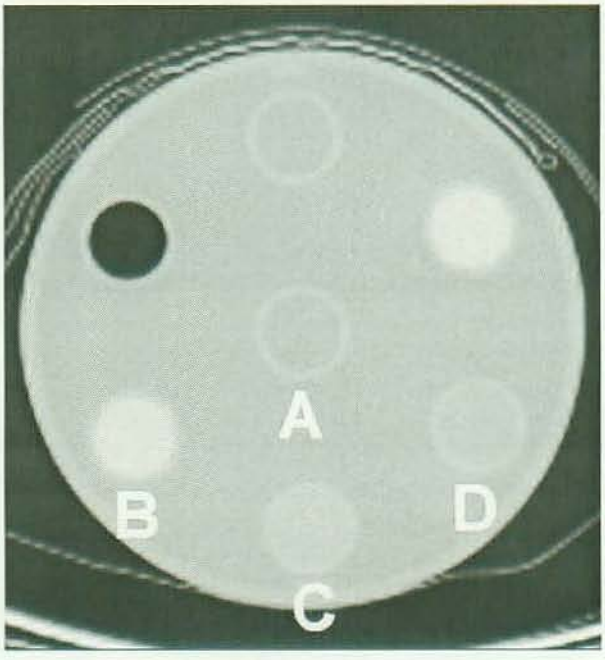

Fig 6. Transaxial CT image of SPECT phantom. Cylinder A contained water and Tl-201. Cylinder B, C, and D contained diluted contrast material at different iodine concentration and Tl-201.

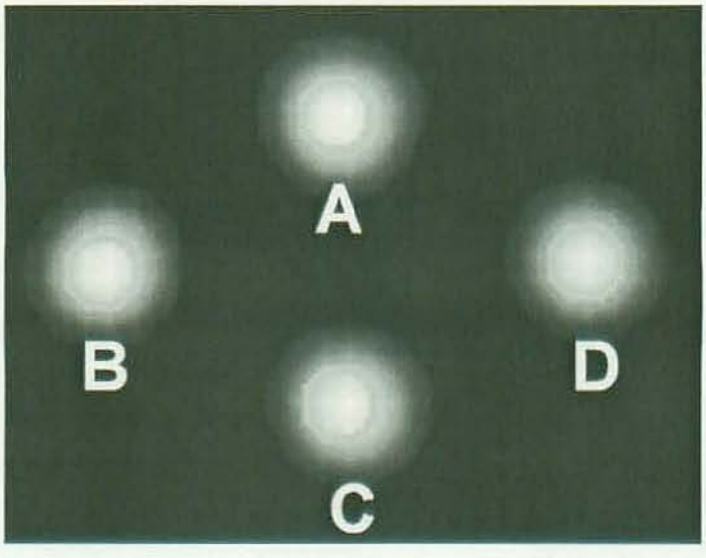

Fig 7. Attenuation-corrected SPECT image by using low-current CT images ($SPECT_{CT10}$).

Section 2: Clinical application of X-ray CT based attenuation correction in myocardial perfusion SPECT imaging

Stress-rest Tl-201 SPECT is a well-established imaging method for evaluating the presence and extent of CAD.(23, 24) However, the diagnostic accuracy of myocardial SPECT is adversely affected by specific physical effects including attenuation, scatter, and blur.(1, 25) Of these, attenuation artifacts are arguably the most serious in the assessment of myocardial perfusion.(1, 25) For non-uniform attenuators like those in the thorax, a patient-specific attenuation coefficient map is necessary.(25, 26) Transmission computed tomography (TCT) with an external gamma-ray source has been proposed(1, 2, 27, 28); however, this method is not widely used in the clinical setting because it yields low-quality TCT images resulting from low photon flux, involves additional expense for software and hardware, and requires longer scan times.(7) While attenuation coefficient maps generated from X-ray CT images(7, 8, 29) represent a simple, potentially useful clinical alternative, only a few studies have addressed the clinical usefulness of patient-specific attenuation correction using X-ray CT images.(7, 8)

In the present study we evaluated the clinical usefulness of X-ray CT based attenuation-corrected SPECT imaging using a SPECT/CT system. We compared myocardial perfusion SPECT images with and without attenuation correction based on the results of coronary angiographs performed for the diagnosis of coronary arterial stenosis.

MATERIALS and METHODS

Patients

Using cases entered into our radiologic database between August 2003 and December 2003, we retrospectively reviewed stress-rest myocardial SPECT images obtained in 30 patients (18 men, 12 women; age 48-79 years; mean age 68 years) who had been examined with our combined SPECT/CT system. All patients referred for stress-rest myocardial SPECT imaging presented with atypical chest pain (n = 18) or were suspected of having myocardial ischemia based on the results of a treadmill exercise test (n = 7) or echocardiography (n = 5). They were recruited based on the following criteria: (a) no known CAD, (b) no coexisting valvular heart disease or cardiomyopathy, and (c) availability of CAG within two weeks after the stress-rest Tl-201 myocardial SPECT and X-ray CT images obtained with a SPECT/CT system. Of the 30 patients, 25 were exercise stress tested; the other 5 underwent pharmacologic stress testing. For emission, 111 MBq (3mCi) of Tl-201 was used in all patients. Imaging began within 15 min after the intravenous injection of Tl-201.

Our institutional review board approved both the multiple imaging studies and the retrospective analyses of these data; the protocol and the types of examinations were explained to all patients and their informed consent was obtained.

Data Acquisition and Processing

We used a SPECT/CT system. The gantry-free SPECT system was a Skylight (ADAC Laboratories). Dual-head detectors were equipped with low-energy, general-purpose parallel-hole collimators; the heads were at 90 degrees to each other. A 30 % window was centered at about 77 keV for the emission data. Projections were digitized onto a 64 x 64 matrix. A total of 32 projections were sampled over 90 degrees

for each detector. Each view was acquired for 60 sec. The eight-row MDCT scanner was a LightSpeed Ultra (General Electric Medical System); the tube voltage was 120 kV, the tube electric current was 20 mA. The slice thickness was 5 mm, the rotation speed 4 sec/rotation under free breathing. The CT dose index (vol) was 6.8 mGy.

Attenuation correction was performed with HYOGO CM software (Hyogo College of Medicine, Nishinomiya, Hyogo) (7) on a Pegasys workstation (ADAC Laboratories). The process of attenuation correction was as follows: 1, image registration of the X-ray CT and SPECT images; 2, a creation of an X-ray CT-derived attenuation map; 3, the SPECT image reconstruction with attenuation correction by means of a ML-EM algorithm. CT slice data were retrieved from an Advantage Windows 4.0P workstation (General Electric Medical System) via DICOM. CT slices were then converted into a SPECT-like data volume (5.9 mm x 5.9 mm x 5.9 mm) for fusion of the SPECT and CT images. Registration of SPECT and CT images was performed manually by use of the margin of the heart as an internal marker by a radiologist, and then the validity of image registration was evaluated on the computer display by two diagnostic radiologists based on consensus. One had nine years experience and the other had 20 years experience in both nuclear medicine and CT imaging. After the CT images were registered with the SPECT images, the CT number was converted into the linear attenuation coefficient (μ) of Tl-201 (73keV) on a pixel-by-pixel basis. The following equation was used for the relationship between CT number and μ (/cm): $\mu = 0.181 \times (CT + 1000) / 1000$.

Using the attenuation coefficient map generated from the CT images, the attenuation-corrected SPECT images were created by the ML-EM method. Transaxial images were reformatted to produce short-axis, vertical long-axis, and horizontal long-axis displays. The reoriented reconstructed data sets and the Bull's eye display

were then used for visual evaluation. For comparison, non-corrected SPECT images were also created by the ML-EM method.

Coronary Angiography

Cardiac catheterization was performed according to standard techniques, with access through the femoral or brachial artery. All segments of the coronary circulation were visualized in at least two projections. The resulting coronary angiograms were evaluated by an angiographer of seven years experience. A notation of abnormal was made when at least one of the three major vascular territories (left anterior descending [LAD], left circumflex [LCX], right coronary artery [RCA]) exhibited luminal narrowing of 50% or greater.

Image Interpretation

Images were viewed on a computer monitor by two readers blinded to the patients' age, and clinical status. Reader 1 had eight years experience and reader 2 had 10 years experience in nuclear cardiology. They were presented both in shades of gray and with a rainbow color scale. Grouped stress and rest studies were presented. The readers interpreted the images for the overall presence of CAD and its presence in each of the 3 main vascular territories (LAD, LCX, or RCA) on a 4-point scale where 1 = normal, 2 = probably normal, 3 = probably abnormal, and 4 = abnormal. Two different reading sessions were held. In the first, non-corrected SPECT images, and in the second, two weeks after the first, attenuation-corrected SPECT images were interpreted. Images were presented in random order to each of the readers at each session. Visual evaluations were performed independently so as to determine interobserver agreement between the two readers. In the absence of consensus, the more severe interpretation was accepted as the final determination. Interobserver variability was assessed with

kappa statistics. Kappa values were reported as follows: 0 = agreement is a random effect: less than 0.20 = poor agreement; 0.21-0.40 = fair agreement; 0.41-0.60 = moderate agreement; 0.61-0.80 = substantial agreement; and 0.81-1.00 = almost perfect agreement.(16) The results of myocardial SPECT imaging were compared with those of CAG. We compared diagnostic accuracy between attenuation-corrected and NC-SPECT images for the overall detection of CAD and for the localized detection of CAD in the LAD, LCX, and RCA territories. We used a scan score of 3 or 4 to indicate abnormal and a score of 1 or 2 to indicate normal in this analysis. McNemar's test was used to analyze the statistical significance of differences in assessing the diagnostic accuracy of each SPECT image. P values of less than 0.05 were considered statistically significant.

RESULTS

Of the 30 patients, 13 had CAD (8 single-vessel, 2 double-vessel, 3 three-vessel CAD). A total of 21 significant stenosis (10 in LAD, 6 in LCX and 5 in RCA, respectively) were present in these patients. The other 17 patients were normal by CAG. Diagnostic accuracy in the detection of coronary arterial stenosis was evaluated for each territory and each patient. Interobserver agreement for visual assessment was substantial or almost perfect. For attenuation-corrected images, the observer consensus for analysis was 0.84 for the LAD-, 0.87 for the LCX-, and 0.71 for the RCA territory. For NC-images, it was 0.91, 0.71, and 0.78. The overall diagnostic accuracy results are presented in Table 1. On attenuation-corrected images, specificity and accuracy were higher than on non-corrected images and the difference in diagnostic accuracy was statistically significant (McNemar test, P = 0.03).

The diagnostic accuracy results in each of three vascular territories are presented in

Table 2. In the RCA territory of the normal subject shown in Fig. 1, attenuation correction yielded improved radioactivity in the inferior wall. Diagnostic accuracy was significantly higher on attenuation-corrected than non-corrected images because of increased specificity in the RCA territory (McNemar test, P = 0.01). In the LAD and LCX territory, there was no significant difference between attenuation-corrected and non-corrected images.

In 17 normal subjects, the percentages with the presence of artifacts of decreased tracer activities were 35% (6/17) and 12% (2/17), respectively, for non-corrected and attenuation-corrected images. For non-corrected images, artifactual decreased perfusion was observed in the RCA- (5/6) and LAD territories (1/6). For attenuation-corrected images, artifactual decreased perfusion was observed in the RCA- (1/2) and LAD territories (1/2).

DISCUSSION

Non-uniform attenuation correction is important in efforts to improve image quality and quantification measurements in myocardial perfusion SPECT imaging.(1, 7, 30, 31) In X-ray CT based attenuation correction, anatomically accurate image registration between SPECT and CT is essential.(7, 8) Our imaging system that combines a gantry-free gamma camera with a 8-row MDCT scanner allows for accurate image fusion between SPECT and CT. Compared to simultaneous transmission methods that employ external sources or hybrid scanners, the primary advantage of our SPECT/CT system is its ability to obtain high-quality anatomical images simultaneously. MDCT is a promising method for the non-invasive visualization of coronary arteries.(32) Image fusion of myocardial perfusion SPECT- and coronary CT angiographic images will be

important in future nuclear cardiology because it features both non-uniform attenuation correction and image fusion functions.

In our study, the increased accuracy of disease localization on attenuation-corrected images resulted from an increase in the specificity in the RCA territory. Comparison of attenuation-corrected and non-corrected images disclosed no changes in the specificity in the LAD or LCX territories. Ohyama et al.(30) evaluated the clinical usefulness of attenuation correction for Tl-201 myocardial SPECT imaging using a three-detector SPECT system equipped with a Tc-99m line source and fan-beam collimators. Our results were similar to theirs, although our study population was relatively small. We suggest that X-ray CT based attenuation correction is also useful in clinical practice. Vidal et al.(33) reported that the increase in specificity obtained with attenuation correction in the RCA territory was accompanied by a significant decrease in the sensitivity of defect detection in the LAD territory. A decrease in sensitivity in the LAD territory on attenuation-corrected images was not observed in this study. However, there was decreased tracer uptake in the LAD territory on the attenuation-corrected but not the non-corrected image in one normal subject on CAG. Reconstructed counts are artificially enhanced in the regions of high tissue density when scattered events are not removed from the projections prior to attenuation correction (30, 34). This may be one of the main reasons why a decrease in activity appears in the LAD territory with attenuation correction. We postulate that over-correction of the inferior wall resulted in a relative decrease in tracer distribution in the LAD territory and we recommend the combined interpretation of attenuation-corrected and non-corrected images. Furthermore, the addition of scatter correction may reduce the drawback of over-correction of the inferior wall (35).

There are several limitations in our study. First, the conversion from CT values to the attenuation coefficient of gamma rays is complex because the energy spectrum of gamma rays is finite while X-rays are continuous. Second, our SPECT images were not scatter-corrected which would have improved image quality and the accuracy of quantification (36, 37). Hendel et al.(38) reported that while the specificity was significantly improved with attenuation/scatter correction and resolution compensation, the detection of coronary artery stenosis was similar on corrected and uncorrected perfusion data. Additional scatter and resolution compensation are desirable to avoid over-correction of the inferior wall that results in a relative decrease in tracer distribution in the LAD territory. Third, quantitative analysis was not performed in this study, because visual assessment of myocardial perfusion images is common in clinical practice. Fourth, we generated SPECT images with 180-degree data collection, chosen because anterior 180-degree acquisition is the standard in the clinical setting (39) . Comparison between 180- and 360-degree acquisitions should be conducted. Fifth, the combined SPECT/CT system is not commonly used due to its increased cost and comparative lack of availability. In recent years, there has been considerable progress in the development of fusion software to co-register different imaging modalities.(40) The development of improved software algorithms is necessary to facilitate automatic and robust image fusion.

In conclusion, the diagnostic accuracy of the localization of CAD was higher on X-ray CT based attenuation-corrected images than non-corrected images as evidenced by an increase in the specificity in the RCA territory. However, X-ray CT based attenuation-corrected and NC-images did not differ significantly with respect to their diagnostic performance in the LAD or LCX territories. These preliminary data suggest

that X-ray CT based attenuation correction in myocardial SPECT imaging has the potential to develop into a reliable clinical technique.

Additional studies are underway in our laboratory to test the usefulness of fusion imaging between myocardial attenuation-corrected SPECT and coronary angiographic MDCT images.

Table 1. Overall diagnostic accuracy for AC- and NC-images

Sensitivity	Specificity	Accuracy
AC 16/21 (76%)	64/69 (93%)	80/90 (89%)
NC 14/21 (67%)	59/69 (86%)	73/90 (81%)

Note. AC = attenuation correction, NC = non correction

Table 2. Diagnostic accuracy for AC- and NC-images in each of three vascular territories.

(LAD)

Sensitivity	Specificity	Accuracy
AC 8/10 (80%)	18/20 (90%)	26/30 (87%)
NC 7/10 (70%)	19/20 (95%)	26/30 (87%)

(LCx)

Sensitivity	Specificity	Accuracy
AC 4/6 (67%)	23/24 (96%)	27/30 (90%)
NC 3/6 (50%)	23/24 (96%)	26/30 (87%)

(RCA)

Sensitivity	Specificity	Accuracy
AC 4/5 (80%)	23/25 (92%)	27/30 (90%)
NC 4/5 (80%)	17/25 (68%)	21/30 (73%)

Note. AC = attenuation correction, NC = non correction.

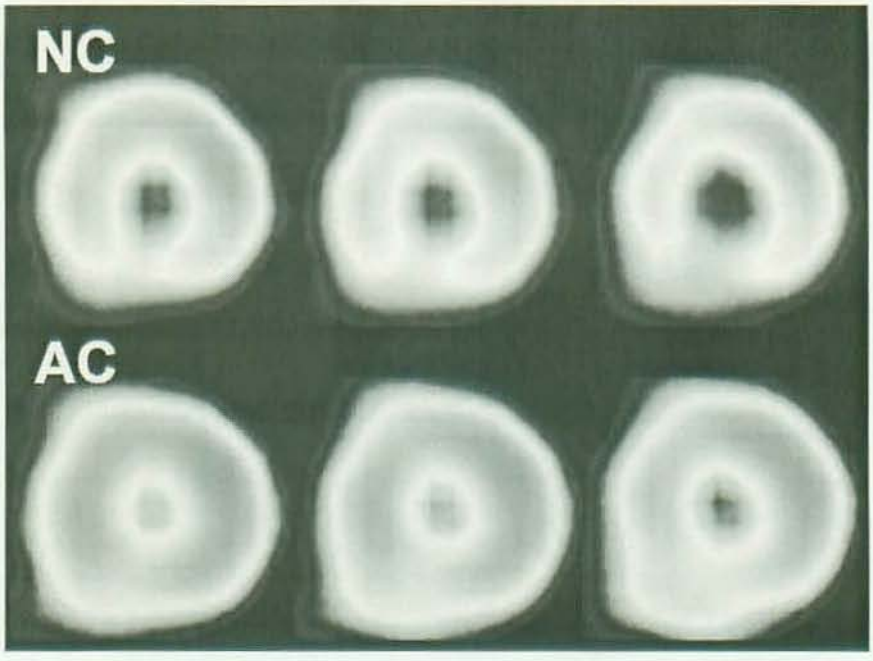

Fig 1.

Short-axial images of a 63-year-old female with normal coronary artery. In non-corrected images (upper), RCA territory shows decreased tracer uptake artifact. In attenuation-corrected images (lower), RCA territory shows normal perfusion.

Section 3. MDCT and QGS for the assessment of LV function

Assessment of both myocardial perfusion and coronary arteries is essential for the diagnosis, management, and follow-up of patients with CAD. Furthermore, the ventricular volume is an independent predictor of morbidity and mortality in these patients (41, 42), and the accurate determination of the LVEF is clinically important (43).

For assessment of the LV function, left ventriculography is the modality of reference, but it is invasive. Echocardiography is non-invasive method, but it may be difficult to perform in obese patients or in those with pulmonary disease or may miss the measurement. Gated cardiac SPECT imaging using the quantitative gated SPECT (QGS) software package is a non-invasive and well-established method for simultaneously studying myocardial perfusion and LV function parameters (44-49). An inherent problem in using QGS is the low spatial resolution (approximately 15 mm) that results in overestimation of LVEF in small hearts (50, 51). MDCT with retrospective electrocardiogram (ECG) gating is a promising tool for coronary artery imaging (32, 52-54). Because data are acquired continuously throughout the entire cardiac cycle, additional end-systolic (ES) and end-diastolic (ED) images can be reconstructed easily from MDCT data sets to analyze cardiac function (55-59). Juergens et al (57) demonstrated a reasonable correlation of LV parameters attained with both MDCT and biplanar cineventriculography. The assessment of volumetric LV parameters based on MDCT imaging appears feasible, however further analysis that compares MDCT and

gated SPECT results seems warranted. Difficulties involve the quality of the data used for comparison in the attempt to compare variables that may change interindividually, and intraindividually from day to day, and to evaluate the interdependence of the changing variables.

In a mechanical phantom, on the other hand, the LV parameters are given and measurements can be repeated. The purpose of the present study was to compare MDCT and QGS results with reference parameters in the assessments of the LV function using an ECG-gated physical cardiac phantom.

MATERIALS AND METHODS

Configuration of the cardiac physical phantom

The design of the cardiac phantom used (Dynamic Cardiac Phantom; Data Spectrum Corporation, Hillsborough, NC) is shown in Figs 1. A cardiac insert, representing the LV, fitted into the adaptation of an anthropomorphic torso phantom. A motor-driven cam moved a piston back and forth to vary LV volumes. The cardiac phantom control unit supplied the power for the electric motor; at each volume cycle it received a signal from the motor to generate a simulated ECG signal that was then transferred to a standard ECG monitor of both the SPECT and MDCT scanners. The LV motion of this cardiac phantom mimicked a clinical stroke volume curve. For each volume cycle, a sensor viewing the motor started the generation of an ECG signal that was synchronized with the cam rotation. The simulated ECG signal was used for gated SPECT and MDCT acquisition. The cardiac phantom controller allowed for two different cycle frequency settings of the motor motion (48 and 77 beats per minute [bpm]), resulting in two different LV stroke volumes. The stroke volume was adjusted and the fixed ESV produced two different volume combinations (Table 1). We actually measured the phantom dimensions. The fixed ESV of the cardiac phantom was 42 ml; this physical phantom simulated a small human heart with ESV of <50 mL. An expansion membrane, incorporated into the base of the torso phantom, allowed for expansion and contraction of the total volume within the anthropomorphic torso phantom during each volume cycle. As this cardiac phantom featured no metal parts, it could be scanned with both SPECT and CT scanners. The inner and outer walls of the simulated LV consisted of two flexible rubber membranes. The compartment between the inner and outer membranes represented the myocardial wall: it was filled with

thallium-201 (0.05 MBq/ml). We chose thallium-201 for our phantom study because thallium-201 myocardial SPECT imaging was routinely used at our hospital to assess myocardial perfusion. The volume within the inner membrane simulated the LV cavity; it was filled with water. We chose water, not contrast media, within the simulated LV cavity because we considered that contrast media potentially cause attenuation artifact on SPECT images. Two radiologists consensually verified that the contrast between the inner membrane and the water in the LV cavity was distinct on CT images and that they could delineate the endocardial contour. One radiologist had 10 years and the other had 8 years of experience in CT imaging.

SPECT/CT

The combined SPECT/CT system incorporated a gantry-free SPECT scanner and a MDCT scanner; both were commercial instruments. The gantry-free SPECT system was a Skylight (ADAC Laboratories), the eight-row MDCT scanner a LightSpeed Ultra (General Electric Medical System). Both commercial devices were juxtaposed so that the CT table could move the cardiac phantom directly into the SPECT scanner prior to CT scanning without the necessity of changing the position of the phantom.

SPECT imaging

Dual-head detectors were equipped with low-energy, general-purpose parallel-hole collimators; the heads were at 90 degrees to each other. The 35% window was centered at about 74 keV for the emission data; projections were digitized onto a 64 × 64 matrix, zoom 1.42 (spatial resolution, 13mm). A total of 32 projections were sampled over 90 degrees for each detector; each view was acquired for 60 sec. SPECT images were reconstructed by filtered back projection, high-frequency noise levels were decreased with post-reconstruction Butterworth filtering (cutoff = 0.50 cycle/pixel, order = 5) on a

Pegasys workstation (ADAC Laboratories). Each R-R interval of the ECG signal was divided into 16 equal time intervals. Thus, temporal resolution of QGS was 78msec/frame and 49msec/frame, respectively, in settings 1 and 2.

CT imaging

The CT parameters for setting 1 (48bpm) were 0.5-sec rotation time, a helical pitch of 0.275:1, 300 mA, and 120 kVp. The CT parameters for setting 2 (77bpm) were 0.6-sec rotation time, a helical pitch of 0.3:1, 300mA, and 120 kVp. Two scans were performed for each setting. One scan was performed with 8 × 1.25-mm collimation, and reconstructed with 2.5-mm slice thickness and 2.5-mm increment. Another scan was performed with 8 × 2.5-mm collimation, and reconstructed with 5.0-mm slice thickness and 5.0-mm increment. CT images were reconstructed using a standard convolution kernel (STD) with a 512 × 512 matrix; the field-of-view was 360 mm; the in-plane spatial resolution was 0.70 mm in each setting. A half reconstruction and a segmental reconstruction algorithm were applied, respectively, in settings 1 and 2. As the use of a segmental reconstruction algorithm was clinically important for cardiac CT imaging in patients with a high heart rate (58, 60), the segment reconstruction algorithm was chosen in setting 2 with the higher heart beat rate. The segment reconstruction algorithm was not applied in setting 1. The temporal resolution was 330 msec and 210 msec, respectively, in settings 1 and 2. Using the ECG trace, phase images were acquired retrospectively starting from early systole (0% of the R-R interval) and ending at the end of diastole (95% of the R-R interval) by using 5%; thus, 20 heart phases were obtained.

Volumetric analysis

For gated measurements with SPECT and MDCT imaging, the volume in the LV

cavity was measured at two different settings (Table 1). To verify the inter-study reproducibility and reliability of the phantom results, each scan was repeated three-times. The coefficient of variation (CoV) for volume measurements of QGS and CT was calculated as the SD of the measured volumes divided by its mean value and then multiplied by 100 to convert to a percentage.

In QGS analysis, the Cedars-Sinai program was used to calculate the EF, ED volume (EDV), and ES volume (ESV) of the ventricle. The Cedars-Sinai method identified myocardial boundaries by asymmetric Gaussian fitting to three-dimensional count profiles of myocardial intensities (61). Using the automatic algorithm, the endocardial and epicardial contours were identified as the points of 65% SD of the count profiles for each of the 16 sets of short-axis slices in the cardiac cycle to calculate volume changes. The largest and smallest LV volumes corresponded to the EDV and ESV, respectively. ED and ES short-axis and vertical long-axis images were displayed, which the radiologist could accept or redraw as necessary. The radiologist had 20 years experience in nuclear cardiology.

In MDCT ventriculography, measurements of the LV volume were performed on images with different reconstructed slice thickness (2.5 mm and 5.0 mm); they are designated CT-2.5 and CT-5.0, respectively. We performed a short-axial image series including 20 heart phases through the entire cardiac cycle at the mid-ventricular level on a dedicated workstation (Advantage Windows 4.0P, GE) in order to visually determine the maximal systolic constriction phase and diastolic phase as the images showing the largest and smallest LV cavity area, respectively. The LV boundaries of the transaxial CT images in the ED and ES phases were delineated manually to yield three-dimensional volume-rendered images by the same radiologist who had 9 years

experience in CT imaging. Then, EDV and ESV were calculated using a software tool on a workstation by summarizing by Simpson method all LV cavities using the manually delineated transaxial slices of ED and ES phases. The EF was calculated from EDV and ESV. The difference between true and measured volumes as a percentage of the true volume was calculated according to the equation: 100 x (Vm – Vt) / Vt (%), where Vm and Vt indicate the measured and true ventricular volume, respectively. Then, the differences in the true and measured volumes were compared among CT-2.5, CT-5.0 and QGS volumetry.

Statistical analysis

One-way ANOVA was used to test the statistical significance of CoV for QGS, CT-2.5, and CT-5.0 volumes. One-way ANOVA was used to test the statistical significance of the difference between the measured and true LV volumes for QGS, CT-2.5, and CT-5.0 images. If there were statistically significant differences, the Tukey-Kramer multiple comparisons test was then applied for post hoc analysis. P values of less than 0.05 were considered to be statistically significant. All data are presented as the mean ± SD. Statistical analyses were performed with a statistical software package (StatView, version 5.0; SAS Institute, Cary, NC).

RESULTS

The measured ventricular volumes and the differences in true and measured volumes as a percentage of the true volume for ventricular volume settings 1 and 2 are shown in Tables 2 and 3, respectively. Transaxial CT images and three-dimensional CT ventriculograms in the ED and ES phases are shown in Fig 2. The three-dimensional volume-rendered images obtained from the QGS program for a 16-frame gated SPECT

study are presented in Fig 3. At each ventricular volume setting, the difference between true and measured ESV and EF values was significantly different. Application of the Tukey-Kramer test revealed that the differences in true and measured values for ESV and EF obtained with QGS were significantly greater than those obtained by CT-2.5 and CT-5.0 volumetry at each ventricular volume setting (Table 4). The difference between true and measured EDV obtained with CT-2.5 was significantly greater than that obtained with CT-5.0 volumetry at volume setting 2.

At ventricular volume settings 1 and 2, the CoV of EDV for QGS was 0.6% and 0.7%, respectively. The corresponding CoV of ESV for QGS was 8.8% and 1.9%. The CoV of EDV for CT-2.5 was 2.8% and 1.6%, respectively at ventricular volume settings 1 and 2. The corresponding CoV of ESV for CT-2.5 was 1.6% and 5.8%. The CoV of EDV for CT-5.0 was 5.2% and 3.9%, respectively, for ventricular volume settings 1 and 2. The corresponding CoV of ESV for CT-5.0 was 7.4% and 5.1%. The difference in the CoV among QGS, CT-2.5, and CT-5.0 was not statistically significant (p=0.37).

DISCUSSION

Retrospective gated MDCT and myocardial SPECT imaging provide anatomical and physiologic information, respectively, and both techniques can be used to estimate LV function (55-59). The diagnostic and prognostic knowledge derived from an understanding of LV function can be added to information gained from assessing myocardial perfusion and coronary artery images. However, in clinical practice there is often a discrepancy between LV volumes measured by MDCT and QGS techniques. Most methods implemented on commercial SPECT systems use edge-detection schemes in the calculation of the EF. Edge-detection schemes are especially susceptible to

partial-volume effects, which become more severe in small hearts. Thus, we considered that the analysis in a small heart was important and the small heart model (the fixed ESV value of 42 mL) was adopted in the study. Our results show that functional and temporal information yielded by coronary MDCT study can be used to obtain a correct estimation of LV function. At an ESV of <50 mL, our cardiac physical phantom produced an overestimation of the EF by QGS analysis of a small heart. Ventricular volume estimations from both QGS and MDCT analyses were highly reproducible; the CoV was 1–9%. We postulate that the artifactual EF increase is attributable to the low spatial resolution (approximately 15 mm) in myocardial SPECT imaging. As the endocardial edges at opposite sides of the LV cavity overlap in the QGS program, the position of the calculated edge is closer to the center of the cavity. This presents a problem for the configuration of ES, especially in cases where the heart is small, because at that point the LV volume is at its lowest and the endocardial edges are at their closest proximity.

Pratt et al. (62) reported that a significant problem when measured with the QGS software lies in the partial-volume effect and the inaccurate determination of the inner boundary at the apex on ES images. Ford et al. (63) found that QGS analysis overestimated EF by 15-25% in simulated small hearts. As our results appear to support their findings, it may be inadvisable to use QGS for monitoring the EF in patients with small hearts. Our data suggest that a mildly decreased EF may appear to be in the normal range when measured by QGS software. On the other hand, MDCT volumetric measurements were highly accurate and reproducible even in small hearts because of the higher spatial resolution (60). Vera et al. (64) reported that QGS underestimated EF by underestimating EDV in patients with large myocardial infarcts: using regression

analysis, they demonstrated that the difference between the results of left ventriculography and QGS volumes was correlated with the size of the infarct. We postulate that the MDCT volume is accurate in patients with myocardial infarction, although further studies are required. We note a tendency of the CT-2.5 volumetry to overestimate the LV volumes as well as a tendency of the CT-5.0 volumetry to underestimate the LV volumes at the higher heart rate setting. We posit that the partial volume effect and the higher heart rate decrease the accuracy of manual tracing of the endocardial contours. Although we found no significant difference in reproducibility between CT-2.5 and CT-5.0 volumetries, the CoV of CT-2.5 volumetry tended to be smaller than of CT-5.0 volumetry. Thus, thin-section image thickness may be preferable for MDCT volumetry.

Myocardial function is widely assessed with the use of echocardiography which is operator- and acoustics-dependent; volumetric assessment is based on geometric assumptions (65, 66). Yamamuro et al. (58) reported that functional analysis with MDCT was more accurate than with two-dimensional echocardiography. Radionuclide ventriculography is flawed due to its low spatial resolution (67, 68), and other parameters that pertain to the myocardial wall are not considered. Therefore, this technique is not widely used. Due its high accuracy and reproducibility cardiac cine MRI with steady-state free precession acquisition is nowadays judged as the state-of-the-art method for assessing the LV function as well as the myocardial perfusion (69, 70). Further improvements are achieved by MR-tagging (71). However, cardiac MRI is a more complex technique and therefore acquisition time is usually longer in comparison to cardiac MDCT. Images acquired with both techniques must be analyzed in postprocessing procedures to attain the LV parameters. Retrospective gated

MDCT is a widely available, accurate and reproducible approach to comprehensively assess the coronary arteries as well as the LV function (52, 58, 72, 73). Our imaging system that combines a gantry-free gamma camera with a MDCT scanner allows for accurate registration between SPECT and high-quality CT images. Image fusion of myocardial perfusion SPECT and coronary CT angiographic images will be important in future cardiology because it features both non-uniform attenuation correction and image fusion functions (8, 74). We believe that the combination of noninvasive coronary artery imaging and the assessment of LV myocardial perfusion and function is an interesting approach to a comprehensive cardiac workup.

There are some limitations in our study. First, as the cardiac phantom was confined to two settings (48 and 77 bpm), we were not able to evaluate the effect of temporal resolution on our volumetric analyses. In general, a beta-blocker is administered orally one hour prior to cardiac CT scanning for patients with a heart rate of greater than 65 beats per minute (75, 76). We considered that the frequency setting of 48 bpm (setting 1) was representative of a patient in whom a beta-blocker was administered, and the frequency setting of 77 bpm (setting 2) was representative of a patient in whom a beta-blocker was contraindicated. However, our phantom study was not designed with the case of heart rate fluctuation during scan. Second, the phantom resembled the human heart's anatomy, but had some deficits of its anatomical specifics, e.g. the papillary muscles and the moving mitral and aortic valve. In the previous report (57), papillary muscles were included in the LV cavity in LV functional analysis. We believe that the measurement error due to some deficits of the anatomical specifics may be small, and our experimental results may be similar to those of a human heart. Third, we did not perform comparisons between combinations of tracer and processing

algorithms. We chose thallium-201 for our phantom study because thallium-201 myocardial SPECT imaging is routinely used at our hospital to assess myocardial perfusion. Earlier validation studies (77, 78) found a good correlation with EF that was independent of the combination of tracer and processing-algorithms. We suggest that our results will not be affected in a major way by other combinations of tracer and processing-algorithms. Fourth, 1.25-mm thin sections were not used for MDCT ventriculography. Grude et al (79) adopted 1.25-mm thin sections for the functional analysis. The use of thin sections may be preferable. However, automated software for cardiac functional analysis has not been optimized, and the manual delineation of LV cavities should be performed. Thus, we considered the use of 1.25-mm thin sections was time-consuming and might limit the clinical use of this technique. Thus, we chose the 2.5-mm and 5.0-mm reconstructed images for the study. Improved software algorithms are imperative to enable automatic and accurate functional analysis.

In conclusion, we found that MDCT provides for good visualization of the morphology and a good estimation of LV function parameters, and that QGS overestimates EF for the small heart model with an ESV of <50 mL as well as normal or near normal LV function. These data argue against using QGS EF for monitoring the EF in patient with small hearts.

Table 1. The two different volume settings used for the true left ventricular volumes in the cardiac physical phantom.

	Cycle frequency (bpm)	EDV (ml)	ESV (ml)	EF (%)
Setting 1	48	100	42	58
Setting 2	77	87	42	52

Table 2. Measured ventricular volumes and difference between true and measured volumes as a percentage of the true volume with SPECT and MDCT volumetry at volume setting 1 (EDV = 100mL; ESV = 42mL; EF = 58%)

	Measurement	EDV (ml)	ESV (ml)	EF (%)
QGS	1	101 (1.0)	28 (-33.3)	72 (24.6)
	2	101 (1.0)	29 (-31.0)	71 (22.9)
	3	100 (0.0)	33 (-21.4)	67 (15.5)
	Mean ± SD	101 ± 1(0.7±0.6)	30 ± 3 (-28.6±6.3)	70 ± 3 (21.0±4.8)
CT-2.5	1	109 (8.9)	43 (1.6)	61 (4.9)
	2	104 (4.3)	41 (-1.4)	61 (3.9)
	3	103 (3.4)	42 (-1.0)	60 (3.1)
	Mean ± SD	106 ± 3 (5.5±2.9)	42 ± 1 (-0.3±1.6)	60 ± 1 (4.0±0.9)
CT-5.0	1	107 (7.0)	43 (2.9)	60 (2.8)
	2	97 (-2.9)	40 (-5.3)	59 (1.8)
	3	106 (5.6)	37 (-11.2)	65 (11.5)
	Mean ± SD	103 ± 5 (3.2±5.4)	40 ± 3 (-4.5±7.1)	61 ± 3 (5.4±5.4)

Note___Three measurements were performed for each method. Data are presented by the measured value (difference between true and measured volumes as a percentage of the true volume [%]).

CT-2.5 = MDCT volumetry with 2.5-mm reconstructed slice thickness, CT-5.0 = MDCT volumetry with 5.0-mm reconstructed slice thickness.

Table 3. Measured ventricular volumes and difference between true and measured volumes as a percentage of the true volume with SPECT and MDCT volumetry at volume setting 2 (EDV = 87mL, ESV = 42mL, EF = 52%)

	Measurement No	EDV (ml)	ESV (ml)	EF (%)
QGS	1	87 (0.0)	31 (-26.2)	64 (24.5)
	2	86 (-1.1)	31 (-26.2)	64 (23.7)
	3	86 (-1.1)	30 (-28.6)	65 (26.0)
	Mean ± SD	86 ± 1 (-0.8±0.7)	30 ± 1(-27.0±1.4)	64 ± 1 (24.7±1.1)
CT-2.5	1	91 (4.9)	44 (3.9)	52 (0.9)
	2	89 (2.4)	43 (2.0)	52 (0.4)
	3	92 (5.7)	39 (-6.9)	57 (11.1)
	Mean ± SD	91 ± 2 (4.3±1.7)	42 ± 2 (-0.3±5.7)	54 ± 3 (4.2±6.1)
CT-5.0	1	83 (-4.9)	41 (-1.5)	50 (-3.3)
	2	89 (1.8)	37 (-11.1)	58 (11.9)
	3	83 (-4.5)	40 (-5.7)	52 (1.2)
	Mean ± SD	85 ± 3 (-2.5±3.8)	39 ± 2 (-6.1±4.8)	53 ± 4 (3.3±7.8)

Note___Three measurements were performed for each method. Data are presented by the measured value (difference between true and measured volumes as a percentage of the true volume [%]).

CT-2.5 = MDCT volumetry with 2.5-mm reconstructed slice thickness, CT-5.0 = MDCT volumetry with 5.0-mm reconstructed slice thickness.

Table 4. Intermodality comparisons of the EDV, ESV, and EF volumetry using MDCT and SPECT at the volume setting 1 and 2.

	Setting 1			Setting 2		
	EDV	ESV	EF	EDV	ESV	EF
CT-2.5 vs CT-5.0	NS	NS	NS	S	NS	NS
CT-2.5 vs QGS	NS	S	S	NS	S	S
CT-5.0 vs QGS	NS	S	S	NS	S	S

Note____CT-2.5 = MDCT volumetry with 2.5-mm image thickness, CT-5.0 = MDCT volumetry with 5.0-mm image thickness, NS = not significant, S = significant ($p<0.05$ for multiple comparisons)

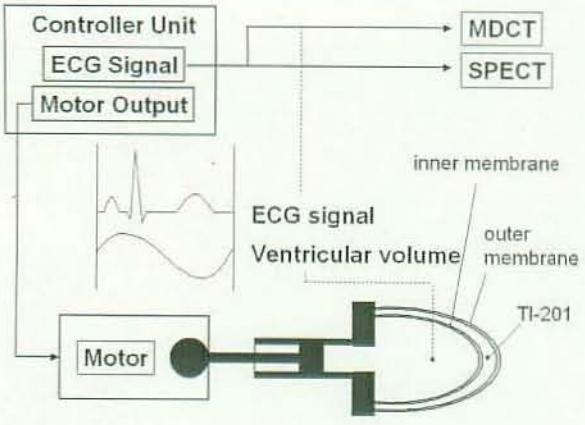

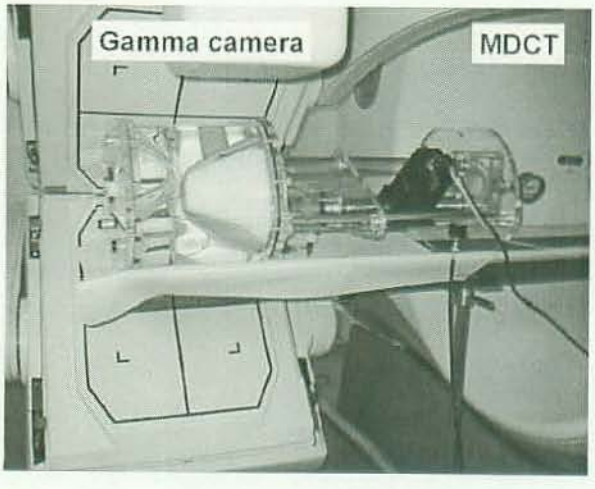

Fig 1.

The scheme of the gated cardiac physical phantom (upper). At each volume cycle a sensor produces a signal to start generation of the ECG signal. The ECG signal is coupled to the LV volume curve. The photograph of the cardiac physical phantom scanned with a combined SPECT/CT system (lower). The cardiac insert, representing LV, fits into the adaptation of the anthropomorphic torso phantom. The imaging table from CT scanner extends into the gantry-free SPECT system.

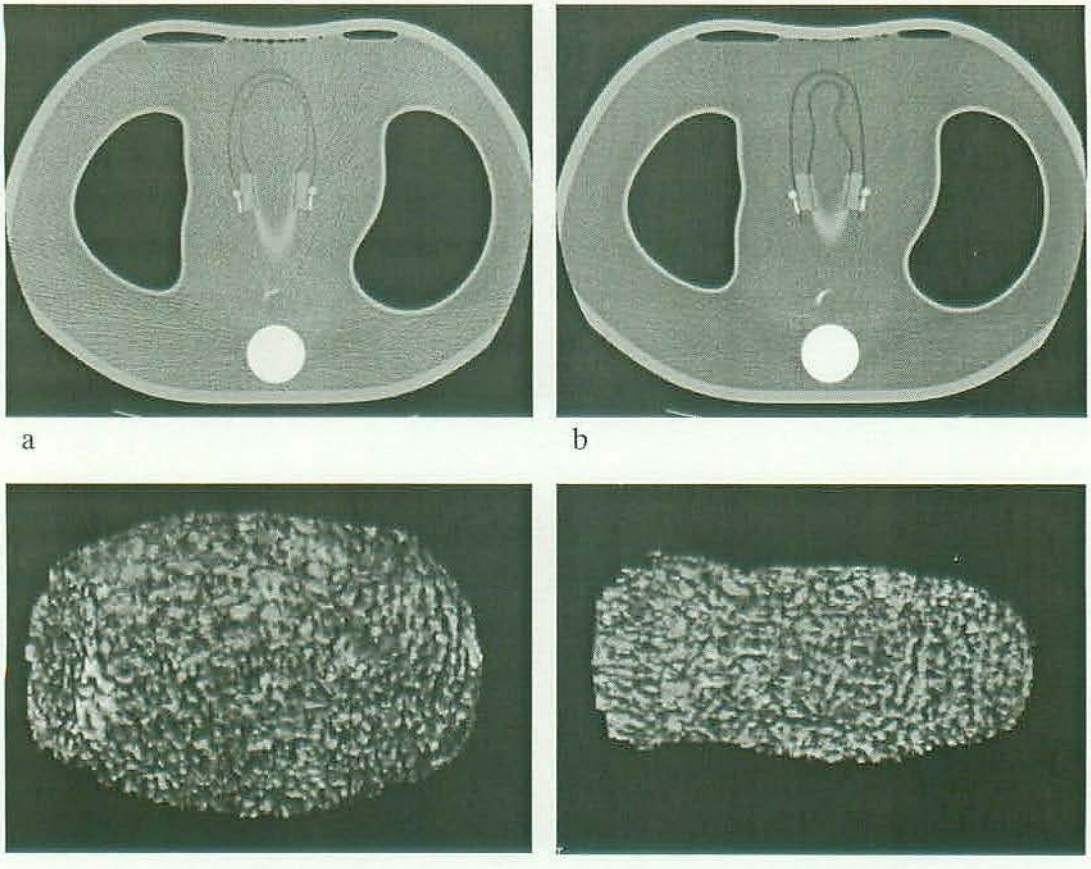

a b

c d

Fig 2. a, b: Transaxial CT images of the cardiac physical phantom in the ED (a) and ES phases (b). c, d: Three-dimensional CT ventriculograms in the ED (c) and ES phases (d).

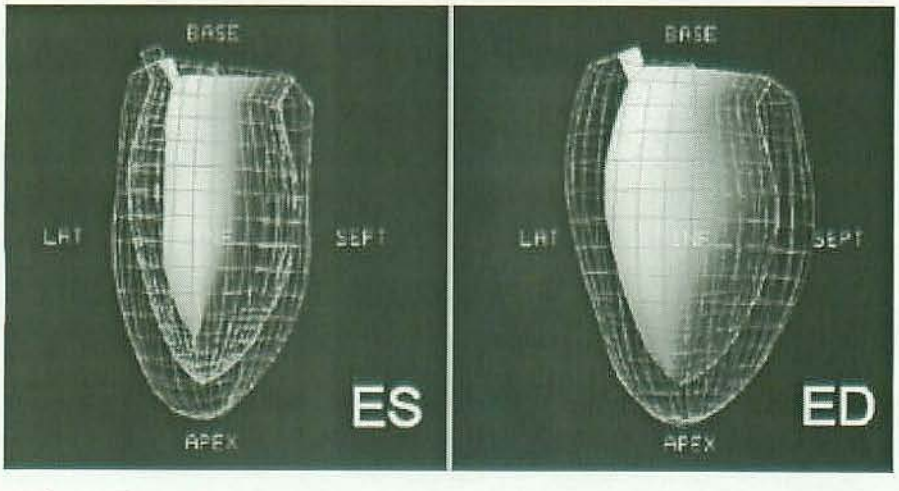

Fig.3. Three-dimensional volume-rendered images obtained from the QGS program.

References

1. Tsui BM, Gullberg GT, Edgerton ER, et al. Correction of nonuniform attenuation in cardiac SPECT imaging. J Nucl Med 1989; 30:497-507.
2. Ficaro EP, Fessler JA, Ackermann RJ, Rogers WL, Corbett JR, Schwaiger M. Simultaneous transmission-emission thallium-201 cardiac SPECT: effect of attenuation correction on myocardial tracer distribution. J Nucl Med 1995; 36:921-931.
3. DePuey EG, 3rd. How to detect and avoid myocardial perfusion SPECT artifacts. J Nucl Med 1994; 35:699-702.
4. Hashimoto J, Ogawa K, Kubo A, et al. Application of transmission scan-based attenuation compensation to scatter-corrected thallium-201 myocardial single-photon emission tomographic images. Eur J Nucl Med 1998; 25:120-127.
5. Prvulovich EM, Lonn AH, Bomanji JB, Jarritt PH, Ell PJ. Effect of attenuation correction on myocardial thallium-201 distribution in patients with a low likelihood of coronary artery disease. Eur J Nucl Med 1997; 24:266-275.
6. Hasegawa BH, Lang TF, Brown JK, et al. Object-specific attenuation correction of SPECT with correlated dual-energy X-ray CT. IEEE Trans Nucl Sci 1993; 40:1242-1252.
7. Kashiwagi T, Yutani K, Fukuchi M, et al. Correction of nonuniform attenuation and image fusion in SPECT imaging by means of separate X-ray CT. Ann Nucl Med 2002; 16:255-261.
8. Takahashi Y, Murase K, Higashino H, Mochizuki T, Motomura N. Attenuation correction of myocardial SPECT images with X-ray CT: effects of registration errors between X-ray CT and SPECT. Ann Nucl Med 2002; 16:431-435.

9. LaCroix KJ, Tsui BMW. Hasegawa BH, Brown JK. Investigation of the use of X-ray CT images for attenuation compensation in SPECT. IEEE Trans Nucl Sci 1994; 41:2793-2799.

10. Bocher M, Balan A, Krausz Y, et al. Gamma camera-mounted anatomical X-ray tomography: technology, system characteristics and first images. Eur J Nucl Med 2000; 27:619-627.

11. Delbeke D, Martin WH, Patton JA. Sandler MP. Value of iterative reconstruction, attenuation correction, and image fusion in the interpretation of FDG PET images with an integrated dual-head coincidence camera and X-ray-based attenuation maps. Radiology 2001; 218:163-171.

12. Goerres GW, Burger C, Kamel E, et al. Respiration-induced attenuation artifact at PET/CT: technical considerations. Radiology 2003; 226:906-910.

13. Goerres GW, Kamel E, Heidelberg TN, Schwitter MR, Burger C, von Schulthess GK. PET-CT image co-registration in the thorax: influence of respiration. Eur J Nucl Med Mol Imaging 2002; 29:351-360.

14. Beyer T, Antoch G, Blodgett T, Freudenberg LF, Akhurst T, Mueller S. Dual-modality PET/CT imaging: the effect of respiratory motion on combined image quality in clinical oncology. Eur J Nucl Med Mol Imaging 2003; 30:588-596.

15. Goerres GW, Kamel E, Seifert B, et al. Accuracy of image coregistration of pulmonary lesions in patients with non-small cell lung cancer using an integrated PET/CT system. J Nucl Med 2002; 43:1469-1475.

16. Svanholm H, Starklint H, Gundersen HJ, Fabricius J, Barlebo H, Olsen S. Reproducibility of histomorphologic diagnoses with special reference to the

kappa statistic. Apmis 1989; 97:689-698.

17. Brown KA. The role of stress redistribution thallium-201 myocardial perfusion imaging in evaluating coronary artery disease and perioperative risk. J Nucl Med 1994; 35:703-706.

18. Singer ME, Applegate KE. Cost-effectiveness analysis in radiology. Radiology 2001; 219:611-620.

19. Weissman IA, Dickinson CZ, Dworkin HJ, O'Neill WW, Juni JE. Cost-effectiveness of myocardial perfusion imaging with SPECT in the emergency department evaluation of patients with unexplained chest pain. Radiology 1996; 199:353-357.

20. Patton JA, Delbeke D, Sandler MP. Image fusion using an integrated, dual-head coincidence camera with X-ray tube-based attenuation maps. J Nucl Med 2000; 41:1364-1368.

21. Balter JM, Ten Haken RK, Lawrence TS, Lam KL, Robertson JM. Uncertainties in CT-based radiation therapy treatment planning associated with patient breathing. Int J Radiat Oncol Biol Phys 1996: 36:167-174.

22. Updated imaging guidelines for nuclear cardiology procedures. part 1. J Nucl Cardiol 2001; 8:G5-G58.

23. DePasquale EE, Nody AC, DePuey EG, et al. Quantitative rotational thallium-201 tomography for identifying and localizing coronary artery disease. Circulation 1988; 77:316-327.

24. Mahmarian JJ, Boyce TM, Goldberg RK, Cocanougher MK, Roberts R, Verani MS. Quantitative exercise thallium-201 single photon emission computed tomography for the enhanced diagnosis of ischemic heart disease. J Am Coll

Cardiol 1990; 15:318-329.

25. Kojima A, Tomiguchi S, Kawanaka K, et al. Attenuation correction using asymmetric fanbeam transmission CT on two-head SPECT system. Ann Nucl Med 2004; 18:315-322.

26. Tung CH, Gullberg GT. A simulation of emission and transmission noise propagation in cardiac SPECT imaging with nonuniform attenuation correction. Med Phys 1994; 21:1565-1576.

27. Jaszczak RJ, Gilland DR, Hanson MW, Jang S, Greer KL, Coleman RE. Fast transmission CT for determining attenuation maps using a collimated line source, rotatable air-copper-lead attenuators and fan-beam collimation. J Nucl Med 1993; 34:1577-1586.

28. Ficaro EP, Fessler JA, Rogers WL, Schwaiger M. Comparison of americium-241 and technetium-99m as transmission sources for attenuation correction of thallium-201 SPECT imaging of the heart. J Nucl Med 1994; 35:652-663.

29. Fleming JS. A technique for using CT images in attenuation correction and quantification in SPECT. Nucl Med Commun 1989; 10:83-97.

30. Ohyama Y, Tomiguchi S, Kira T, et al. Diagnostic accuracy of simultaneous acquisition of transmission and emission data with technetium-99m transmission source on thallium-201 myocardial SPECT. Ann Nucl Med 2001; 15:21-26.

31. Duvernoy CS, Ficaro EP, Karabajakian MZ, Rose PA, Corbett JR. Improved detection of left main coronary artery disease with attenuation-corrected SPECT. J Nucl Cardiol 2000; 7:639-648.

32. Schoenhagen P, Halliburton SS, Stillman AE, et al. Noninvasive imaging of coronary arteries: current and future role of multi-detector row CT. Radiology

2004; 232:7-17.

33. Vidal R, Buvat I, Darcourt J, et al. Impact of attenuation correction by simultaneous emission/transmission tomography on visual assessment of 201Tl myocardial perfusion images. J Nucl Med 1999; 40:1301-1309.

34. Meikle SR, Hutton BF, Bailey DL. A transmission-dependent method for scatter correction in SPECT. J Nucl Med 1994; 35:360-367.

35. Harel F, Genin R, Daou D, et al. Clinical impact of combination of scatter, attenuation correction, and depth-dependent resolution recovery for (201)Tl studies. J Nucl Med 2001; 42:1451-1456.

36. Khalil ME, Brown EJ, Jr., Heller EN. Does scatter correction of cardiac SPECT improve image quality in the presence of high extracardiac activity? J Nucl Cardiol 2004; 11:424-432.

37. Kojima A, Kawanaka K, Nakaura T, et al. Attenuation correction using combination of a parallel hole collimator and an uncollimated non-uniform line array source. Ann Nucl Med 2004; 18:385-390.

38. Hendel RC, Berman DS, Cullom SJ, et al. Multicenter clinical trial to evaluate the efficacy of correction for photon attenuation and scatter in SPECT myocardial perfusion imaging. Circulation 1999; 99:2742-2749.

39. DePuey EG, Garcia EV. Updated imaging guidelines for nuclear cardiology procedures. Part 1. J Nucl Cardiol 2001; 8:G1-G58.

40. Townsend DW, Cherry SR. Combining anatomy and function: the path to true image fusion. Eur Radiol 2001; 11:1968-1974.

41. Hammermeister KE, DeRouen TA, Dodge HT. Variables predictive of survival in patients with coronary disease. Selection by univariate and multivariate

analyses from the clinical, electrocardiographic, exercise, arteriographic, and quantitative angiographic evaluations. Circulation 1979; 59:421-430.

42. White HD, Norris RM, Brown MA, Brandt PW, Whitlock RM, Wild CJ. Left ventricular end-systolic volume as the major determinant of survival after recovery from myocardial infarction. Circulation 1987; 76:44-51.

43. The-Multicenter-Postinfarction-Research-Group. Risk stratification and survival after myocardial infarction. N Engl J Med 1983; 309:331-336.

44. Bavelaar-Croon CD, Kayser HW, van der Wall EE, et al. Left ventricular function: correlation of quantitative gated SPECT and MR imaging over a wide range of values. Radiology 2000; 217:572-575.

45. Atsma DE, Bavelaar-Croon CD, Germano G, et al. Good correlation between gated single photon emission computed myocardial tomography and contrast ventriculography in the assessment of global and regional left ventricular function. Int J Card Imaging 2000: 16:447-453.

46. Germano G, Kavanagh PB, Kavanagh JT, Wishner SH, Berman DS, Kavanagh GJ. Repeatability of automatic left ventricular cavity volume measurements from myocardial perfusion SPECT. J Nucl Cardiol 1998; 5:477-483.

47. Germano G. Automatic analysis of ventricular function by nuclear imaging. Curr Opin Cardiol 1998; 13:425-429.

48. Maunoury C, Chen CC, Chua KB, Thompson CJ. Quantification of left ventricular function with thallium-201 and technetium-99m-sestamibi myocardial gated SPECT. J Nucl Med 1997; 38:958-961.

49. Maunoury C, Antonietti T, Sebahoun S, Barritault L. Assessment of left ventricular function by 201Tl SPECT using left ventricular

cavity-to-myocardium count ratio. Nucl Med Commun 2001; 22:281-285.

50. Feng B, Sitek A, Gullberg GT. Calculation of the left ventricular ejection fraction without edge detection: application to small hearts. J Nucl Med 2002; 43:786-794.

51. Toba M, Kumita S, Cho K, et al. Comparison of Emory and Cedars-Sinai methods for assessment of left ventricular function from gated myocardial perfusion SPECT in patients with a small heart. Ann Nucl Med 2000; 14:421-426.

52. Nieman K, Oudkerk M, Rensing BJ, et al. Coronary angiography with multi-slice computed tomography. Lancet 2001; 357:599-603.

53. Kopp AF, Schroeder S, Kuettner A, et al. Non-invasive coronary angiography with high resolution multidetector-row computed tomography. Results in 102 patients. Eur Heart J 2002; 23:1714-1725.

54. Rodenwaldt J. Multislice computed tomography of the coronary arteries. Eur Radiol 2003; 13:748-757.

55. Mochizuki T, Murase K, Higashino H, et al. Two- and three-dimensional CT ventriculography: a new application of helical CT. AJR Am J Roentgenol 2000; 174:203-208.

56. Mochizuki T. Koyama Y, Tanaka H, Ikezoe J, Shen Y, Azemoto S. Images in cardiovascular medicine. Left ventricular thrombus detected by two- and three-dimensional computed tomographic ventriculography: a new application of helical CT. Circulation 1998; 98:933-934.

57. Juergens KU, Grude M, Fallenberg EM, et al. Using ECG-gated multidetector CT to evaluate global left ventricular myocardial function in patients with

coronary artery disease. AJR Am J Roentgenol 2002; 179:1545-1550.

58. Yamamuro M, Tadamura E, Kubo S, et al. Cardiac functional analysis with multi-detector row CT and segmental reconstruction algorithm: comparison with echocardiography, SPECT, and MR imaging. Radiology 2005; 234:381-390.

59. Juergens KU, Maintz D, Grude M, et al. Multi-detector row computed tomography of the heart: does a multi-segment reconstruction algorithm improve left ventricular volume measurements? Eur Radiol 2005; 15:111-117.

60. Begemann PG, van Stevendaal U, Manzke R, et al. Evaluation of spatial and temporal resolution for ECG-gated 16-row multidetector CT using a dynamic cardiac phantom. Eur Radiol 2005; 15:1015-1026.

61. Germano G, Kiat H, Kavanagh PB, et al. Automatic quantification of ejection fraction from gated myocardial perfusion SPECT. J Nucl Med 1995; 36:2138-2147.

62. Pratt J, JL L, Trujillo N. An automated program for LVEF calculation from gated SPECT perfusion data that significantly reduces partial volume errors. J Nucl Med 1999; 40(suppl):176P.

63. Ford PV, Chatziioannou SN, Moore WH, Dhekne RD. Overestimation of the LVEF by quantitative gated SPECT in simulated left ventricles. J Nucl Med 2001; 42:454-459.

64. Vera P, Koning R, Cribier A, Manrique A. Comparison of two three-dimensional gated SPECT methods with thallium in patients with large myocardial infarction. J Nucl Cardiol 2000; 7:312-319.

65. Fortuin NJ, Hood WP, Jr., Craige E. Evaluation of left ventricular function by echocardiography. Circulation 1972; 46:26-35.

66. Schiller NB, Shah PM, Crawford M, et al. Recommendations for quantitation of the left ventricle by two-dimensional echocardiography. American Society of Echocardiography Committee on Standards, Subcommittee on Quantitation of Two-Dimensional Echocardiograms. J Am Soc Echocardiogr 1989; 2:358-367.

67. Ashburn WL, Schelbert HR, Verba JW. Left ventricular ejection fraction--a review of several radionuclide angiographic approaches using the scintillation camera. Prog Cardiovasc Dis 1978; 20:267-284.

68. Lethimonnier F, Furber A, Balzer P, et al. Global left ventricular cardiac function: comparison between magnetic resonance imaging, radionuclide angiography, and contrast angiography. Invest Radiol 1999; 34:199-203.

69. Higgins CB, Sakuma H. Heart disease: functional evaluation with MR imaging. Radiology 1996; 199:307-315.

70. Ichikawa Y, Sakuma H, Kitagawa K, et al. Evaluation of left ventricular volumes and ejection fraction using fast steady-state cine MR imaging: comparison with left ventricular angiography. J Cardiovasc Magn Reson 2003; 5:333-342.

71. Ennis DB, Epstein FH, Kellman P, Fananapazir L, McVeigh ER, Arai AE. Assessment of regional systolic and diastolic dysfunction in familial hypertrophic cardiomyopathy using MR tagging. Magn Reson Med 2003; 50:638-642.

72. Coche E, Vlassenbroek A, Roelants V, et al. Evaluation of biventricular ejection fraction with ECG-gated 16-slice CT: preliminary findings in acute pulmonary embolism in comparison with radionuclide ventriculography. Eur Radiol 2005; 15:1432-1440.

73. Juergens KU, Grude M, Maintz D, et al. Multi-detector row CT of left

ventricular function with dedicated analysis software versus MR imaging: initial experience. Radiology 2004; 230:403-410.

74. Nakaura T, Utsunomiya D, Shiraishi S, et al. Images in cardiovascular medicine. Fusion imaging between myocardial perfusion single photon emission computed tomography and cardiac computed tomography. Circulation 2005; 112:e47-48.

75. Pannu HK, Flohr TG, Corl FM, Fishman EK. Current concepts in multi-detector row CT evaluation of the coronary arteries: principles, techniques, and anatomy. Radiographics 2003; 23 Spec No:S111-125.

76. Nieman K, Cademartiri F, Lemos PA, Raaijmakers R, Pattynama PM, de Feyter PJ. Reliable noninvasive coronary angiography with fast submillimeter multislice spiral computed tomography. Circulation 2002; 106:2051-2054.

77. Cho K, Kumita S. [Clinical application of left ventricular volume and ejection fraction derived from gated SPECT data]. Kaku Igaku 2002; 39:97-102.

78. Germano G, Erel J, Kiat H, Kavanagh PB, Berman DS. Quantitative LVEF and qualitative regional function from gated thallium-201 perfusion SPECT. J Nucl Med 1997; 38:749-754.

79. Grude M, Juergens KU, Wichter T, et al. Evaluation of global left ventricular myocardial function with electrocardiogram-gated multidetector computed tomography: comparison with magnetic resonance imaging. Invest Radiol 2003: 38:653-661.